Rev.Adv.Mater.Sci. 18(2008) 18-22

FATIGUE CHARACTERISTICS OF A ZR-BASED BULK METALLIC GLASS

G. Y. Wang[1], P. K. Liaw[1,*], A. Smyth[2], M. Denda[2], A. Peker[3], M. Freels[1], R. A. Buchanan[1] and C. R. Brooks[1]

[1]Department of Materials Science and Engineering, The University of Tennessee, Knoxville, TN 37996, USA
[2]Department of Mechanical & Aerospace Engineering, The State University of New Jersey, Rutgers, NJ 08854, USA
[3]LiquidMetal Technologies Inc., Lake Forest, CA 92630, USA

Received: March 29, 2008

Abstract. High-cycle fatigue (HCF) experiments were conducted on $Zr_{41.2}Ti_{13.8}Cu_{12.5}Ni_{10}Be_{22.5}$ bulk-metallic glass (BMG). The cast samples were machined into the notched fatigue specimens whose stress-concentration factor (K_t) is 1.55 of the stress acting over the notched section. The value of K_t was applied to the stress-range value and in good agreement with the numerical value obtained by our finite-element analysis (FEA). The fatigue results exhibit the fatigue-endurance limit of $Zr_{41.2}Ti_{13.8}Cu_{12.5}Ni_{10}Be_{22.5}$ to be about 30 - 40% of the ultimate tensile strength.

1. INTRODUCTION

As an excellent candidate for structural materials, the scientific and technological interests in the bulk-metallic glass (BMG) have been enormous. The mechanical behavior of BMGs has been studied widely [1-6]. However, the fatigue study of BMGs is still scarce and the understanding of their fatigue behavior is poor. The results of 4-point-bend fatigue experiments conducted on Vitreloy 1 beam specimens showed that the fatigue-endurance limits, based on the stress range, were only 6-10% of the ultimate tensile strengths [7-8]. On the other hand, the tension-tension and rotating fatigue experiments performed on Zr-based BMG samples [9-12] exhibit the fatigue-endurance limits as high as 40 - 50% of the ultimate tensile strengths. What is the reason for such a large difference? Many factors could be involved, such as the mean stress, specimen geometry, chemical environment, temperature, cyclic frequency, residual stress, material quality, and surface condition. In fact, any processing that changes the static mechanical properties or microstructures is also likely to affect the fatigue behavior of materials. However, some factors must play a dominant role. The formation of shear bands is still unclear during the cyclic deformation of the BMGs. The initiation and propagation of the fatigue crack in metallic glasses need to be scrutinized. It is necessary to undertake a fundamental study regarding the fatigue behavior of the BMGs.

The button-head fatigue specimens were employed in our experiments [9-11]. The BMG materials are usually brittle. In order to facility the fatigue behavior of the BMGs conveniently, a notch was machined at the middle section of the sample. Thus, the sample will fail at the notched section. The stress-concentration factor (K_t) of 1.55 [9-11] was employed in the stress-range values at the notched section. In this paper, the high-cycle fatigue behaviors of BMGs are studied. A finite-element analysis (FEA) is employed to verify the stress concentration factor of the notched sample.

Corresponding author: P. K. Liaw, e-mail: pliaw@utk.edu

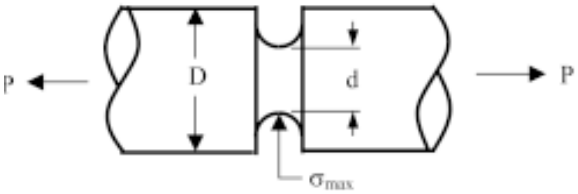

Fig. 1. Schematic of a tension bar sample.

Fig. 2. The 2-D axisymmetric model.

A recent paper [13] reported that the study of the stress state and final fracture surfaces for the notched specimens together with a lower stress-concentration factor [8,14] could lead to much lower fatigue-endurance limits than reported in this paper.

2. EXPERIMENTAL PROCEDURES

The $Zr_{41.2}Cu_{12.5}Ni_{10}Ti_{13.8}Be_{22.5}$ (in atomic percent) samples (LM001) were made by Liquidmetal Technologies, Inc. (Lake Forest, CA). There were two batches of samples from different lots (Batches 59 and 94). Batch 59 contains less oxygen than Batch 94. A computer-controlled Material Test System (MTS) servohydraulic testing machine was employed for fatigue studies. Samples were tested at various stress ranges with a R ratio ($R = \sigma_{min.}/\sigma_{max.}$, where $\sigma_{min.}$ and $\sigma_{max.}$ are the applied minimum and maximum stresses, respectively) of 0.1 under a load-control mode, using a sinusoidal waveform at a frequency of 10 Hz.

ANSYS® (general-purpose FEA software) was used to model the notched bar sample of LM001 and determine the axial stress concentration at the notch tip under the tension loading. An axisymmetric two-dimensional (2-D) model and a three-dimensional (3-D) model were employed to verify the analytical accuracy. The stress-concentration factor (K_n) is, then, calculated by dividing the maximum stress at the root of the notch ($\sigma_{max.}$) by the nominal stress, which can be present if a stress concentration does not occur. Note that K_t and K_n are the stress concentration factors based on the normal stress on the un-notched and nothced cross-sections, respectively (Fig. 1). They are given as follows:

$$K_t = \frac{\sigma_{max.}}{S_t}, \tag{1}$$

$$K_n = \frac{\sigma_{max.}}{S_n}, \tag{2}$$

where $S_t = 4P/\pi d^2$ and $S_n = 4P/\pi D^2$ are the normal stresses on the notched and un-notched cross-sections, respectively, and P is the tensile load. The relationship between K_t and K_n is give by:

$$K_t = K_n \frac{d^2}{D^2}. \tag{3}$$

The BMG material was modeled as a linear isotropic elastic solid. The Young's Modulus (E) and the Poisson's ratio (ν) are the essential material parameters for these models. For $Zr_{41.2}Cu_{12.5}Ni_{10}Ti_{13.8}Be_{22.5}$, E is 96 GPa and n is 0.36 [15].

3. RESULTS AND DISCUSSION

The 2-D axisymmetric model used in ANSYS is shown in Fig. 2. The bottom side of the model has two displacement-boundary conditions ($U_x = U_z = 0$), while the right side of the model has also two displacement-boundary conditions ($U_z = U_y = 0$). The element used in ANSYS is the PLANE83 (8-node quadrilateral and 6-node triangular axisymmetric solid element) element, which supports axisymmetric loads. When meshing the 2-D model, the area near the notch was meshed with triangular elements, which well fit the curved notch boundary. The top portion of the bar was mapped with quadrilateral elements. These two areas were, then, "glued" together so that they formed one entity, as shown in Fig. 3a. After refining the mesh near the notched area, the model is solved with the appropriate loads that result in S_n = 1 MPa. After reading the results, the deformed shape can be plotted as shown in Fig. 3b. A contour figure was plotted to show the axial stress distribution (Fig. 4). Thus, the maximum axial stress of 2.678 MPa can be obtained. Since the nominal stress was of unit magnitude, the stress concentration factor, K_n,

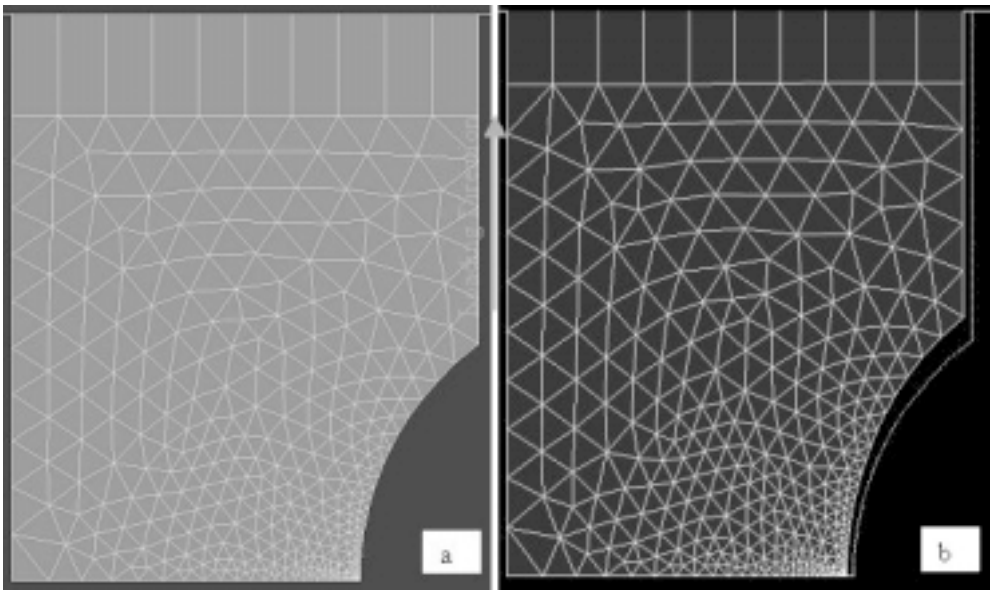

Fig. 3. (a) Meshed 2-D model; (b) deformed shape.

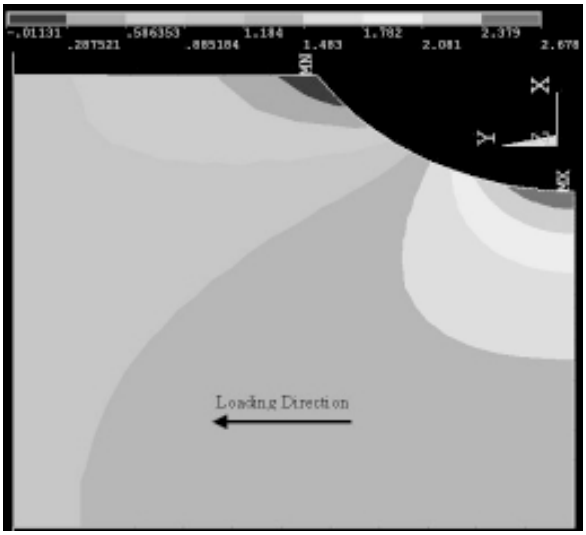

Fig. 4. A contour plot of the axial stress distribution.

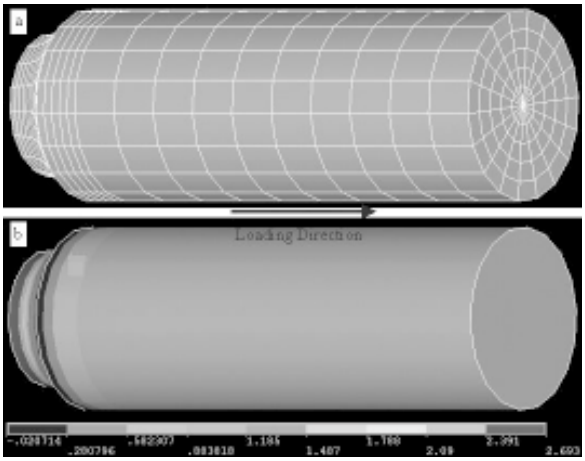

Fig. 5. (a) Meshed 3-D model; (b) a contour plot of the axial stress distribution.

is 2.678 at the notch tip for the 2-D axisymmetric model.

A full 3-D model with appropriate boundary and symmetry conditions was used to solve the same problem. The model is meshed using SOLID95 (3-D 20-node structural solid element) elements and mapped using the VOLUME SWEEP (a command to fill an existing unmeshed volume with elements) option in ANSYS, so the hexagonal elements were formed (Fig. 5a). With this mesh, 3-D wedges were formed, which could cause problems if the stress gradient is too high. Since the sample in our experiment does not have a high stress gradient, these elements are acceptable. After meshing the specimen and applying the same loads as the 2-D model does, the problem was solved. After reading the data, a contour plot of the axial stress was presented in Fig. 5b. The results showed that the maximum stress for the 3-D model was 2.693 MPa. Therefore, the stress concentration factor, K_n, is 2.693.

Based on the calculation of two models, it is reasonable that K_n is considered as 2.69. $K_t = 1.49$ can be obtained using Eq. (3). Fig. 6 shows the previous fatigue results with $K_t = 1.55$ and the current fatigue results with $K_t = 1.49$. When K_t is ap-

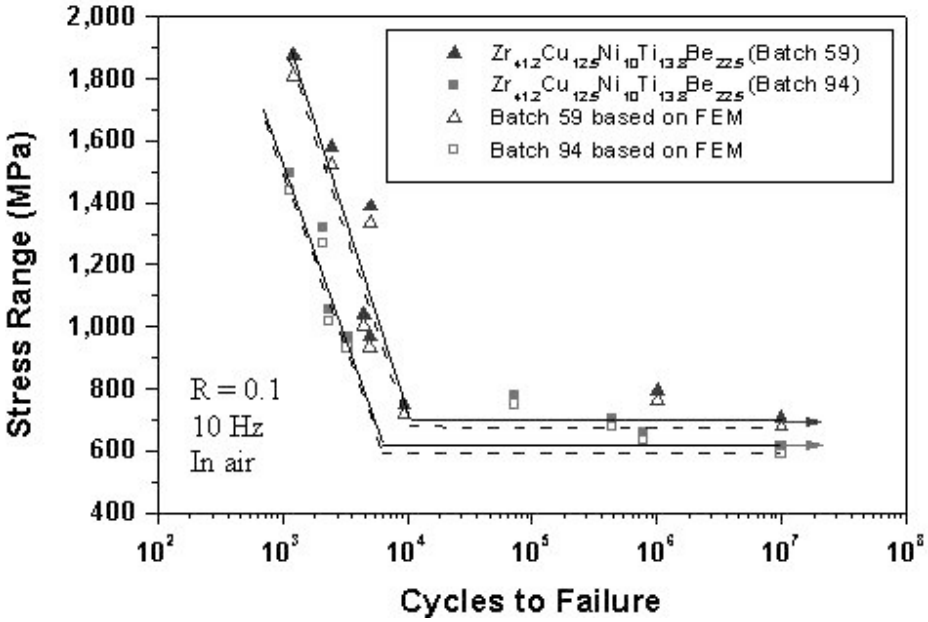

Fig. 6. The comparison of stress-range/fatigue-life data with K_t = 1.55 and K_t = 1.49.

plied as 1.55, the values of the fatigue-endurance limit (σ_e) for the $Zr_{41.2}Cu_{12.5}Ni_{10}Ti_{13.8}Be_{22.5}$ (Batch 94) and $Zr_{41.2}Cu_{12.5}Ni_{10}Ti_{13.8}Be_{22.5}$ (Batch 59) samples subjected to tension-tension loading, based on the stress range, were approximately 615 MPa and 703 MPa, respectively, and the fatigue ratios (σ_e divided by the ultimate tensile strength) for Batch 94 and Batch 59 were 0.33 and 0.38, based on the ultimate tensile strength of 1,850 MPa and 1,850 MPa, respectively. [16]. If K_t = 1.49 is used now, the fatigue-endurance limits for Batch 94 and Batch 59 are 591 MPa and 676 MPa, respectively, and the fatigue ratios for Batch 94 and Batch 59 were 0.32 and 0.37, respectively. The difference between the previous results and the current results is about 4%. Therefore, it is acceptable that the stress-concentration factor (K_t) of 1.55 was employed in the stress-range values at the notched specimens in the previous papers [9-11,16]. After fatigue testing, the fractured surfaces of all samples were observed by the scanning-electron microscopy (SEM). The investigation revealed that the crack initiated from the outer surface of the notch section for all of Batch 59 samples and most of Batch 94 samples. However, for some Batch 94 samples, the crack initiated from the porosity or inclusion inside the sample. Since casting defects, such as porosities and oxide inclusions, exist, the stress concentration could form around these defects. Why did the crack not initiate from the outer surface of the notch section since the maximum stress is at the root of the notch section? The possible reason is that the stress near the casting defects inside samples is greater than the maximum stress at the root of notch section. As the large casting defects exist inside Batch 94 samples, which indicate that the sample body is not continuous and isotropic, the current models cannot be used to calculate the stress concentration. The fatigue behavior of Batch 59 was better than that of Batch 94 (Fig. 6) because fewer cracks initiated from porosities and oxide inclusions in Batch 59 [16]. This trend reveals that if there are no obvious casting defects inside BMG materials, the fatigue behavior could be improved further.

4. CONCLUSIONS

The notched-bar sample was simulated by 2-D and 3-D FEM models successfully, and the stress concentration factor at the root of notch section was determined. The results show that it is reasonable that the stress-concentration factor (K_t) of 1.55 was employed to determine the stress-range values of

the fatigue data at the notched specimens in the present research. Batch 59 exhibits better fatigue behavior than Batch 94. The fatigue-endurance limit of LM001 is about 30 - 40% of the ultimate tensile strength.

ACKNOWLEDGEMENTS

We would like to acknowledge the financial support of the National Science Foundation: (1) the Division of the Design, Manufacture, and Industrial Innovation Program, (2) the Combined Research-Curriculum Development Programs, (3) the Integrative Graduate Education and Research Training Program, (4) the International Materials Institutes Program, and (5) the Major Research Instrumentation Program, to the University of Tennessee, Knoxville, with Dr. D. Durham, Ms. M. Poats, Dr. C. J. Van Hartesveldt, Dr. D. Dutta, Dr. W. Jennings, Dr. L. Goldberg, Dr. C. Huber, and Dr. C. R. Bouldin as Program Directors, respectively.

REFERENCES

[1] R.T. Ott, C. Fan, J. Li and T.C. Hufnagel // *Journal of Non-Crystalline Solids* **317** 158 (2003).

[2] G. He, W. Löser, J. Eckert and L. Schultz // *Materials Science and Engineering A* **352** (2003) 179.

[3] H. Choi-Yim, R.D. Conner, F. Szuecs and W.L. Johnson // *Acta Materialia* **50** (2002) 2737.

[4] T. Mukaia, T.G. Nieh, Y. Kawamura, A. Inoue and K. Higashi // *Intermetallics* **10** (2002) 1071.

[5] H. Li, C. Fan, K. Tao, H. Choo and P.K. Liaw // *Advanced Materials* **18** (2006) 752.

[6] C. Fan, H. Li, L.J. Kecskes, K. Tao, H. Choo, P.K. Liaw and C.T. Liu // *Physical Review Letters* **96** (2006) 145506.

[7] C.J. Gilbert, J.M. Lippmann and R.O. Ritchie // *Scripta Materialia* **38** (1998) 537.

[8] P.A. Hess, B.C. Menzel and R.H. Dauskardt // *Scripta Materialia* **54** (2006) 355.

[9] W.H. Peter, P.K. Liaw, R.A. Buchanan, C.T. Liu, C.R. Brooks, J.A. Horton, Jr., C.A. Carmichael, Jr. and J.L. Wright // *Intermetallics* **10** (2002) 1125.

[10] G.Y. Wang, P.K. Liaw, W.H. Peter, B. Yang, Y. Yokoyama, M.L. Benson, B.A. Green, M.J. Kirkham, S.A. White, T.A. Saleh, R.L. McDaniels, R.V. Steward, R.A. Buchanan, C.T. Liu and C.R. Brooks // *Intermetallics* **12** (2004) 885.

[11] G.Y. Wang, P.K. Liaw, W.H. Peter, B. Yang, M. Freels, Y. Yokoyama, M.L. Benson, B.A. Green, T.A. Saleh, R.L. McDaniels, R.V. Steward, R.A. Buchanan, C.T. Liu and C.R. Brooks // *Intermetallics* **12** (2004) 1219.

[12] Y. Yokoyama, P.K. Liaw, M. Nishijima, K. Hiraga, R.A. Buchanan and A. Inoue // *Materials Transactions JIM* **47** (2006) 1286.

[13] B.C. Menzel and R.H. Dauskardt // *Scripta Materialia* **55** (2006) 601.

[14] B.C. Menzel and R.H. Dauskardt // *Acta Materialia* **54** (2006) 935.

[15] R.D. Conner, A.J. Rosakis, W.L. Johnson and D.M. Owen // *Scripta Materialia* **37** (1997) 1373.

[16] G.Y. Wang, P.K. Liaw, A. Peker, B. Yang, M.L. Benson, W. Yuan, W.H. Peter, L. Huang, M. Freels, R.A. Buchanan and C.R. Brooks // *Intermetallics* **13** (2005) 429.